Measurements on Long and Rigid Objects for Radar Field Probe

P. S. P. Wei (Retired)

The Boeing Company, Seattle, Washington
paxwei3@gmail.com

Abstract – As a novel concept for field probes, radar cross section (RCS) measurements on long rigid objects rotated within a small angular range in and out of the broadside condition are reported. The rotation was maintained either in a horizontal (H) plane or in a vertical (V) plane containing the center of the quiet-zone (QZ). Processing the RCS data by DFT yields a spectrum, which is recognized as the field distribution along that object. This spectrum compares extremely well to traditional field-probes taken earlier by translating a sphere across the QZ in H- or V-direction. Preliminary results at several S-band frequencies are presented and discussed.

Keywords – Compact range, field distribution, large targets, and RCS measurements.

I. INTRODUCTION

For accurate radar cross section (RCS) measurements, it is important to perform the field probe in the target zone as a function of frequency, polarization, and the locations. Traditionally, one can translate a calibration object (e.g., a sphere) across the test zone, and to analyze the response with respect to the field uniformity or the variation thereof. Such a method is usually time consuming and costly. Besides, the probe and its supporting structure (if large) may often contaminate the very field being probed.

While searching for a suitable calibration object for the cross-polarized channels in the Boeing 9-77 compact range, we studied dielectric strings stretched tightly across the range at 45° from horizontal and near broadside to the radar. The lower end of the string was anchored to the floor while the upper end was tied to the upper turntable (UTT). Rotating the UTT would produce a pattern from the string as a function of the aspect-angle. It dawned on us that when we processed the data by the digital Fourier transform (DFT), it would generate a response spectrum, which was related to the incident wave-field distribution along that string at 45° from horizontal [1, 2].

Of practical interest regarding field probes, the two major orientations are *horizontal* and *vertical* intersecting at the quiet-zone (QZ) center. The problem and challenge for the experiments are to assemble such long and rigid targets, mounting it to the range and maneuvering it for the desired motion. To validate the concept, some preliminary measurements were taken (among others) from a 60-ft steel rod supported *horizontally* [3], and a 40-ft aluminum cylinder plus a blue rope supported *vertically* [4]. The results are analyzed in connection with the feasibility of the new concept.

II. HORIZONTAL MEASUREMENTS

The 60-ft long rod (diameter 1.74 inches) was assembled by connecting six 10-ft long steel conduits together. The five joints were each made by fastening the ends of two adjacent conduits with screws to a short cylindrical stem inserted inside the conduits. The screw-heads were kept flush to the outer surface. The outside of the joints were wrapped with conducting aluminum tape. The two ends of the long rod were each covered by a flat circular plate and then painted. The long rod, weighing 75 pounds, was supported by eight pairs of strings (non-flashing) from the UTT at eight attachment points evenly distributed along its length, as depicted in Fig. 1.

Figure 2 shows the typical azimuth dependence of the radar echoes at 2.4 GHz from the 60-ft long rod. Data have been collected in the range of $\pm$ 20°, but only those within $\pm$ 5° are

Submitted On: Feb. 23, 2013
Accepted On: Aug. 27, 2013

plotted here. The main peak is very narrow. The side-lobes are asymmetric. Note that the VV trace (red) is shifted down by -10 dB to avoid overlap, and that it is very similar to the HH trace (blue).

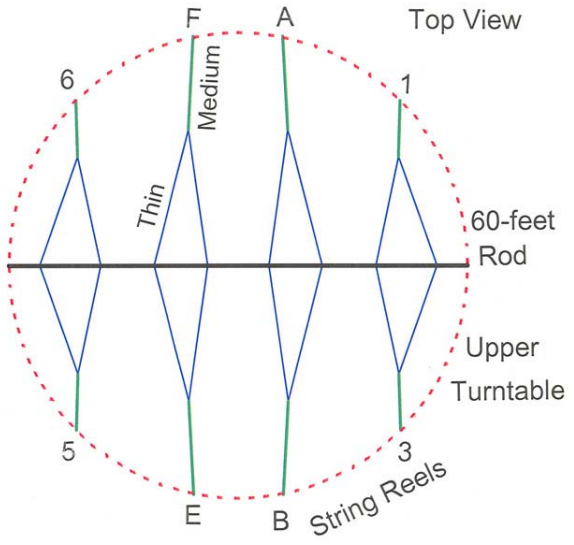

Fig. 1. Schematic of the 60-ft rod supported horizontally by eight string-reels (where A, B, E, F represent high-capacity and 1, 3, 5, 6 represent low-capacity string-reels) from the UTT (of diameter 60 feet, represented by a circle of red dashes).

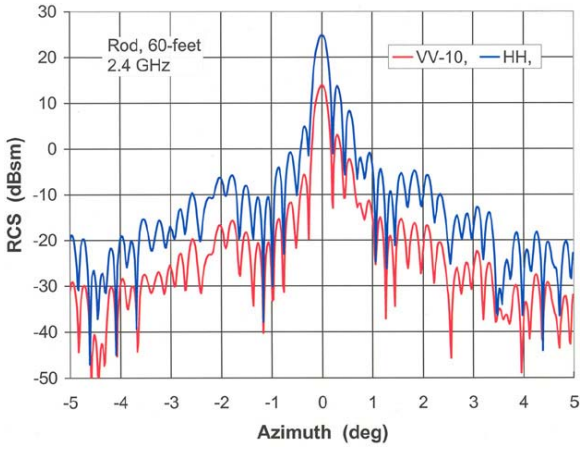

Fig. 2. Azimuth patterns in radar echoes at 2.4 GHz measured from the 60-ft long rod supported horizontally by strings.

Figure 3 shows the Fourier transform spectra using the 2.4 GHz data (of I and Q). The central portion within $\pm$ 800 bins exhibits a plateau at about 35 dB above the noise floor. We recognize that the intensity variation on the plateau is of interest. Though the plateau is fairly flat at the center, it drops off quickly on the two sides. The fast oscillating wiggles near bins $\pm$ 750 are commonly known as the Gibb's phenomenon due to truncation of the rod.

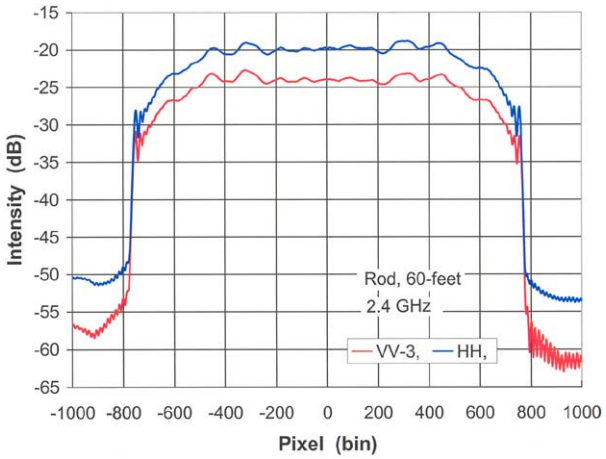

Fig. 3. Typical Fourier transform spectra from the azimuth measurements of the 60-ft rod at 2.4 GHz, (with HH in blue, VV in red and shifted down by -3 dB).

Figure 4 shows extended plots of the two ends, with computed points in symbols. The next step is to calibrate the bin number to distance along the rod. The appropriate formula taken from [1, 2] is as follows,

$$R / \lambda = J * (D_a - 1) / (2W * A * N) \qquad (1)$$

where R is the cross-range distance, $\lambda = c / F$ is the radar wavelength, J is the bin number measured from zero, N = power of 2, zero-padded, is the total size of the data set, D_a is the number of measured data points, A is the UTT-angle swept (in radian), c is the speed of light, and W = 1 here, is a conversion factor which relates the UTT-angle to the actual out-of-plane angle for the rotation (if needed). In equation (1), we find that R and J have a unique relationship, once all the other parameters are known.

For easy comparison with the horizontal field probes using the 14-inch sphere recorded in 1996, we plot the results on similar scales in Fig. 6, i.e., the ordinate in 5 dB/div., the abscissa in 60 inch/div. By aligning Figs. 5 and 6, we can readily discern their strong resemblance, curve by curve,

wiggle by wiggle, per polarization and per frequency. Thus, the 60-ft rod provided the same horizontal field probe results, even at a higher resolution and over a wider coverage area. The close agreement validates the new method of performing field probes as proposed earlier [1, 2]. Furthermore, it is nice to know that the wave-field at the Boeing 9-77 compact range on three arbitrarily chosen frequencies has not changed with time.

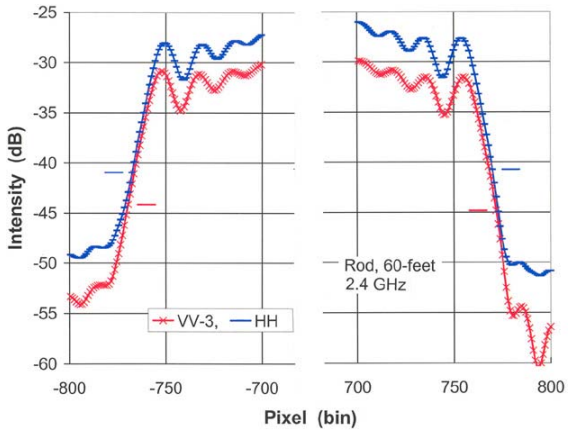

Fig. 4. Extended view of the two ends of the Fourier transform spectra at 2.4 GHz. For calibration of pixel bin versus cross-range distance, the points at -13 dB down from the outermost peaks (denoted by short bars) are taken as end points.

Figure 5 shows the new results from the 60-ft rod of the field distribution represented by the Fourier transform spectra for both HH and VV polarizations at 3 frequencies. The ordinate scale (y-axis) is for the HH trace (blue) at 2.0 GHz, while the HH for 2.4 and 2.8 are shifted down successively by -10 dB. The VV traces (red) are each shifted down by -3 dB from the corresponding HH. We see that the features in Figs. 5 and 6 match each other remarkably well as a function of cross-range distance, per frequency and per polarization.

III. VERTICAL MEASUREMENTS

The configuration of test geometry for moving an object in a vertical plane using the high-capacity string-reels at the 9-77 compact range is shown in Fig. 7 (a) (schematic) and (b) (photograph). The 40-ft aluminum rod (4-inch diameter) supported by a blue rope through its center was the first target for measurement. The angular motion of the rod with respect to the pivot (on top) was achieved by pulling on the weight either by the pair of strings A and F from the front side, or by the pair of strings B and E from the back side. Figure 1 shows the relative placements of the string-reels.

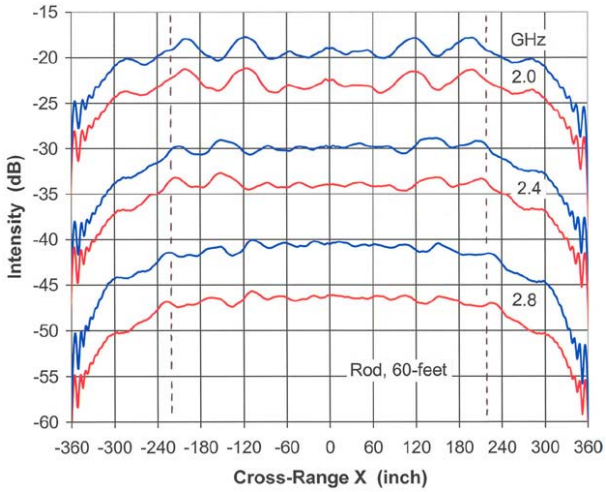

Fig. 5. Fourier transform spectra for the 60-ft rod after calibration of the cross-range distance and at three representative frequencies (2.0 GHz, 2.4 GHz, and 2.8 GHz). Dashed lines mark the boundary of ± 220 inches for easy comparison with the earlier results (see Fig. 6).

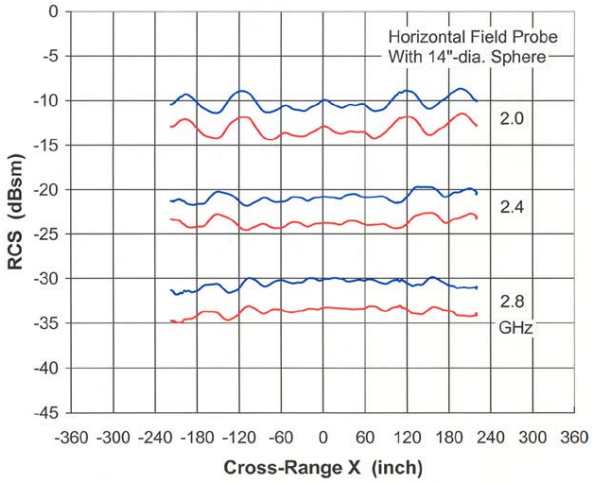

Fig. 6. Horizontal field probes measured in 1996 at three frequencies by translating a 14-inch sphere supported by strings within the distance of ± 220 inches [7].

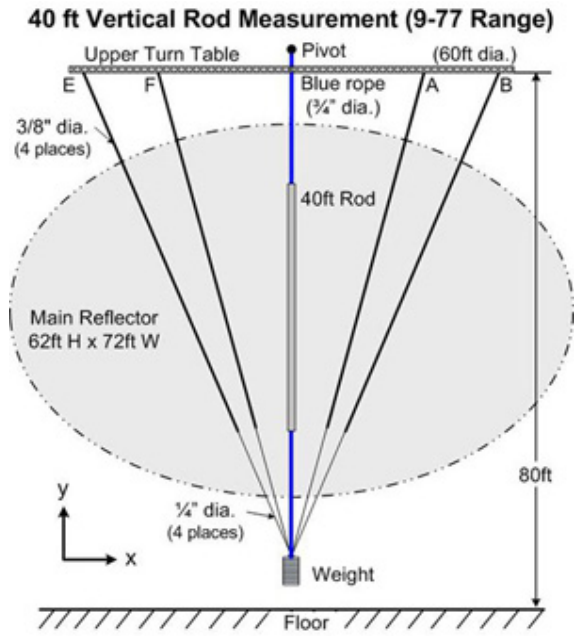

(a)

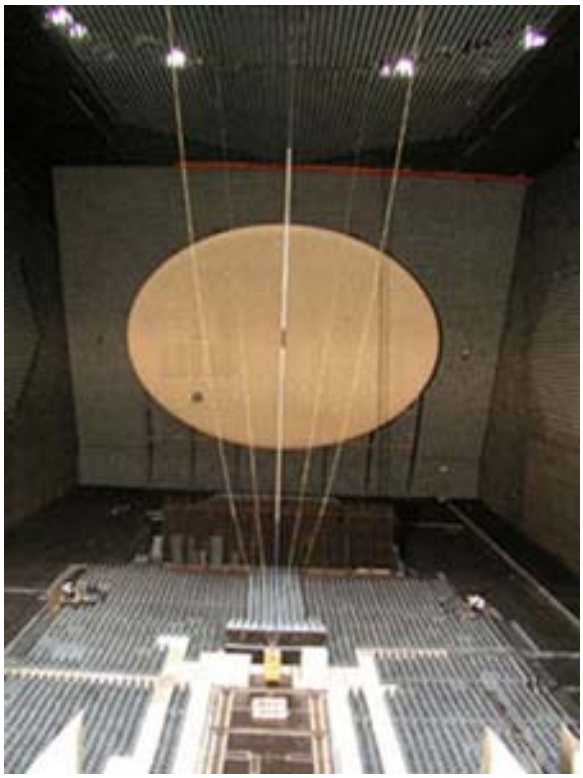

(b)

Fig. 7. (a) Schematic diagram of the test geometry for the vertical measurements and (b) photograph of the test geometry for vertical measurements (as viewed from the back).

The RCS data thus collected as a function of the translation distance of the lower end of the rod along Z (proportional to the out-of-plane tilt angle) were studied and analyzed. The second target was a separate piece of blue rope (dielectric, of 0.75 inch diameter before being stretched). The artesian coordinates (Fig. 7 (a)) are defined according to the right-handed system with the X-axis pointing east, Y-axis pointing up vertically, and the Z-axis pointing out from the page (away from the main reflector, down-range, to the south).

Figures 8 and 9 show the measured radar echoes at 2.4 GHz on the 40-ft rod and on the long blue rope, respectively. They look very similar, except in [dBsm] scale. In Fig. 9, the difference in peak RCS for the blue rope, (VV-HH) at 2.4 GHz, was found to be 6.002 dB. With reference to the wave equations for thin dielectric strings, the ratio of $(T_E / T_H)^2$ for the vertical string gives rise to a simple expression of $\{(\varepsilon_o+1)^2 / 4\}$, where ε_o = 2.99 can be estimated as the dielectric constant of the rope [5, 6]. Also in Fig. 9, the peak RCS for the rope in VV at 2.4 GHz was measured at 7.124 [dBsm]. Though the ka value at 0.479 (for the original radius of 0.375 inch) was moderate, not thin, let us assume that the equation for $S_{vv} = (T_E)^2 = [(L / 2) (\pi)^{1/2} (\varepsilon_o-1) (ka)^2]^2$ may still apply [5, 6]. By using L = 37.66 feet = 11.486 meter, and ε_o = 2.99, we can estimate the ka to be 0.335, or a = 0.262 inch as the "effective" radius of the rope (for wave scattering) after being stretched by a heavy weight.

A retro-reflecting ring was taped to the lower edge of the rod (Y= -20 ft) to facilitate monitoring of its motion by precision optical monitoring system (POMS). The (x, y, z) positions of the marker, recorded along with the radar data, were analyzed. The increments in dz versus z are shown in Fig. 10. Proper application of the DFT algorithm requires that the input data set must be equally spaced. In reality, however, the tilting motion of a vertically positioned object by pulling the strings tied to its lower end was not as smooth as we would have liked. To show how badly the sampling was, we subjected the as-measured raw data (2.4 GHz, VV) to DFT, and we obtained the arbitrary shaped spectra (in black) for the two cases in Fig. 11 (40-ft rod) and Fig. 12 (blue rope). Re-sampling of the raw data in regular steps of 0.20 inch (for increasing z from -60 to 60 inches) was performed by two methods:

a) Linear interpolation using the two nearest neighbors at each z position.

b) Spline interpolation using four data points at each prospective location, (aka cubic spline fit).

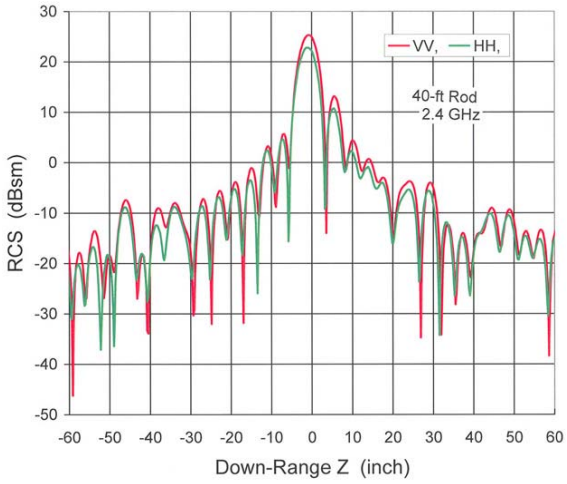

Fig. 8. Radar responses from the vertical 40-ft rod at 2.4 GHz versus distance z. The pattern reached its peak within a narrow range in z when the rod was at broadside to the wave-front.

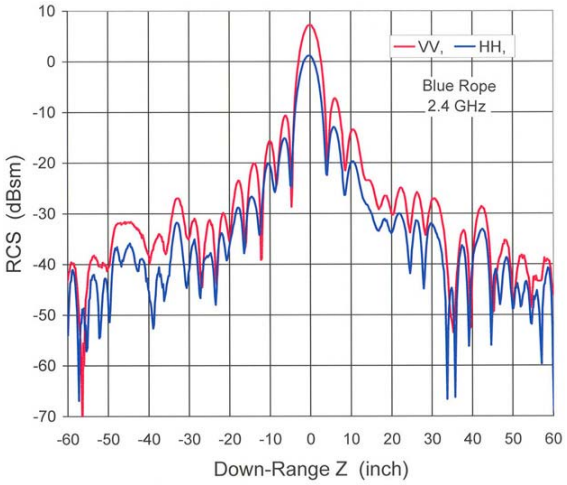

Fig. 9. Radar responses from the vertical blue rope at 2.4 GHz versus distance z. Though similar to Fig. 8 above, the HH scattering from the dielectric rope was weaker than its VV by 6 dB.

In the DFT spectra from the linearly interpolated data for the 40-ft rod (Fig. 11, in green) and for the blue rope (Fig. 12, in blue), we see that the spectra now show an interesting feature consisting of a plateau at about 40 dB above the noise level. The DFT spectra from the spline interpolated data are also plotted (in red) for the two cases. For clarity, the DFT spectra are displaced on the amplitude scale by dB values as noted in the graph. Upon closer inspection, we see that the red spectra exhibit more (or better) fine structures than those from the linearly interpolated data (in green or in blue). Thus, the spline interpolation method was chosen for further analysis in the present work.

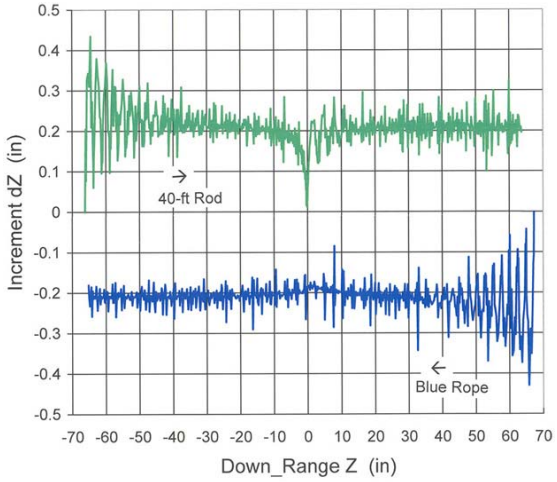

Fig. 10. Motion of z-increments versus z for the 40-ft rod (green) and the blue rope (blue). The direction of motion is indicated by an arrow. Note the swinging motion at the beginning of a run, as well as the hesitation near the broadside at z = 0.

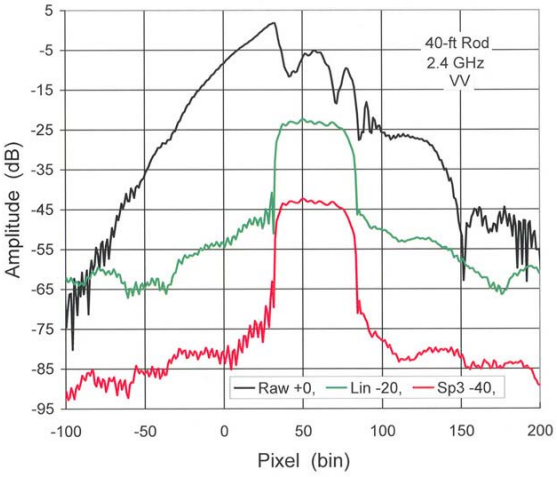

Fig. 11. DFT spectra of the as-measured raw data (black, arbitrarily shaped) and re-sampled data for the 40-ft rod. The stepped plateau was of prime interest in the present work. The cubic spline fit (red) showed more details than the linear interpolation (green).

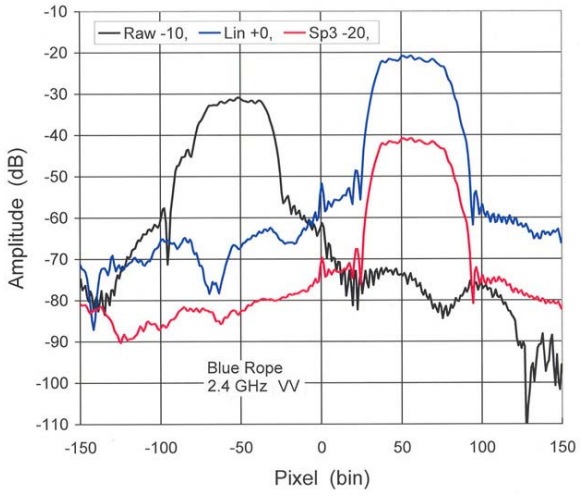

Fig. 12. DFT spectra of as-measured raw data (black) and re-sampled data for the blue rope (otherwise similar to Fig. 11 above).

Calibration of vertical distance Y was facilitated by the Gibb's phenomenon due to the finite length of the 40-ft rod in Fig. 11, plus the small peak at zero pixel due to the pivot of rotation in Fig. 12. The pivot for the swinging motion of the targets was about 4 feet above the UTT (see Fig. 7 (a)). Figure 13 shows the same data at 2.4 GHz (both HH and VV) re-plotted as a function of the abscissa in the calibrated vertical distance Y (in feet). The ripples across the plateau represent the variation in field as sampled from the vertical objects by their small angular motions in a plane containing the YZ-axes. While the 40-ft rod showed abrupt cutoffs, the blue rope by its nearly floor-to-ceiling length (< 80 ft) would actually sample the field tapered much beyond the nominal quiet zone boundary (Y = $\pm$ 14 ft) in the vertical dimension. Except for some minor difference, the field distributions within $\pm$ 14 feet from the center are qualitatively similar as sampled from the two objects, and for each of the two polarizations.

In Figs. 14 and 15, we compare the results of field distributions at three frequencies obtained by the two objects plotted with the same scales. While the VV spectra for both objects are plotted in red, the HH spectra are plotted separately for the 40-ft rod (in green) and the blue rope (in blue) for easy distinction. The abscissae are Y-distance in 10 feet per division. The ordinates are in 3-dB per division, which was calibrated to the [dBsm] scale for the 2.0 GHz VV-case only. The VV traces for the 2.4 GHz and 2.8 GHz are each shifted down by -6 dB from the previous VV trace.

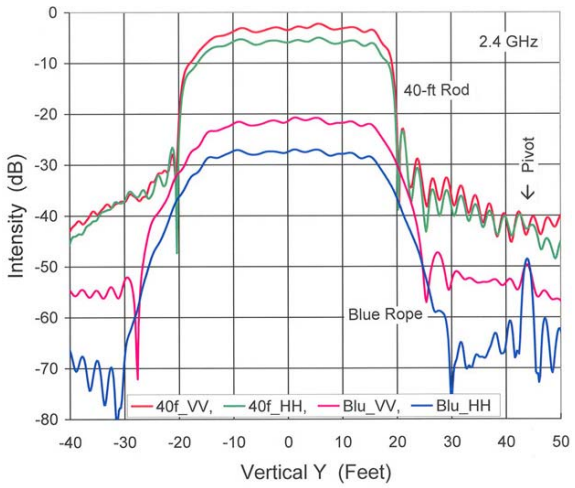

Fig. 13. DFT spectra versus calibrated distance Y for the 40-ft rod and the blue rope at 2.4 GHz for both VV and HH polarizations.

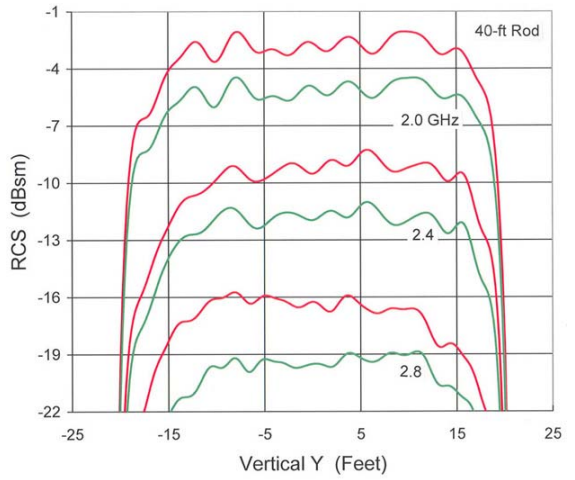

Fig. 14. FFT spectra versus vertical distance from the 40-ft rod at selected frequencies and polarization [VV (red) and HH (green)]. The cutoffs were due to the finite length of the rod.

In Fig. 14, the HH traces are each shifted down by -2 dB from the respective VV at the same frequency. Yet, in Fig. 15, since the HH scattering from the dielectric blue-rope is -6 dB weaker than the corresponding VV, the HH traces are each shifted up by 4 dB from the respective VV, so as to match the appearance of Fig. 14. We see in Figs. 14 and 15 that the DFT spectra obtained from the two different vertical objects (a metal rod

and a dielectric rope) are remarkably similar per frequency and per polarization, but varying in magnitude [dBsm].

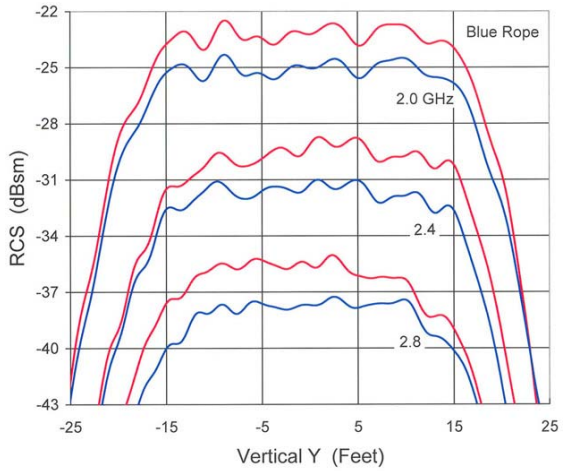

Fig. 15. FFT spectra from the blue rope versus frequency and polarization [VV (red) and HH (blue)]. The results showed a wider field distribution tapering out from the quiet zone boundary. Different only in RCS scale (dBsm) for the two vertical objects, the features of Figs. 14 and 15 (as a representation of field distribution) looked extremely similar.

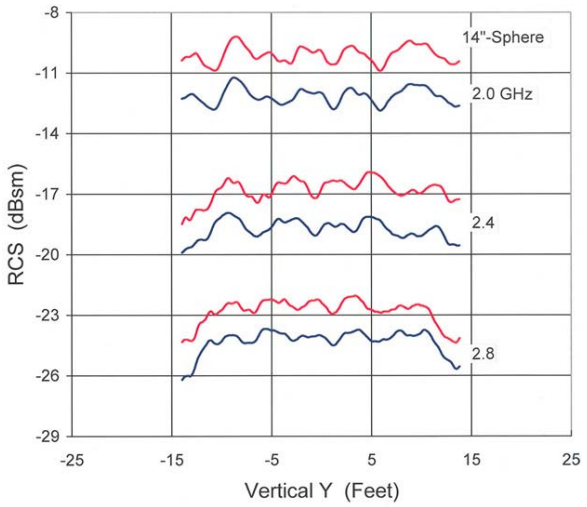

Fig. 16. Vertical field probes by a calibration sphere versus frequency and polarization recorded in 1996 [7]. The quiet zone boundary in the vertical dimension was specified as ± 14 ft, (or ± 168 inches).

For comparison with the new results shown in Figs. 14 and 15, we revisit the field probes measured by translating a sphere supported by strings in the vertical direction through the QZ center, (data collected in 1996). In Fig. 16 (which is plotted with the same scales), we see that the field distributions are very comparable with the new results. It is comforting to know that the radar wave-field has remained about the same with time.

IV. SUMMARY AND CONCLUSION

The measurements described in this paper took a group effort by dedicated colleagues (named in the references) several years to accomplish. To them I am deeply grateful. We conclude that the new method of performing field probes by the angular motion of a long rigid object, in either the horizontal or vertical plane, has been successfully demonstrated and validated. Further research should shed new light on radar measurements.

REFERENCES

[1] P. Wei and E. Knott, "The long string as a field probe," *Proc. 27th AMTA*, pp. 136-141, 2005.

[2] E. Knott and P. Wei, "The long string as a field probe," *IEEE Ant. and Prop. Mag.* , vol. 47, no. 6, pp. 22-27, Dec. 2005.

[3] P. Wei, A. Reed, C. Ericksen, J. Doty, and R. Schuessler, "Field probe from the angular response of a rigid body," *U.S. Patent 7,498,977 issued to the Boeing Company*, March 2009.

[4] P. Wei, A. Reed, C. Ericksen, J. Doty, and R. Schuessler, "Determining characteristics of a radar cross section (RCS) test range," *U.S. Patent 8,098,194 issued to the Boeing Company*, Jan. 2012.

[5] P. Wei, A. Reed, and E. Knott, "Study of wires and strings of finite sizes," *Proc. 20th AMTA*, pp. 221-226, 1998.

[6] E. Knott, A. Reed, and P. Wei, "Broadside echoes from wires and strings," *Microwave Journal*, vol. 42, Horizon House, pp. 102, Jan. 1999.

[7] P. Wei, A. Reed, C. Ericksen, and M. Bushbeck, "Study of RCS measurements from a large flat plate," *Proc. 7th AMTA*, pp. 3-8, 2005. Some typical field-probe results are included in Appendix A: Fig. A1, horizontal; Fig. A2, vertical.

[8] M. Agatonovic, Z. Marinkovic, and V. Markovic, "Application of ANNs in evaluation of microwave pyramidal absorber performance," *Applied Computational Electromagnetics Society (ACES) Journal*, vol. 27, no. 4, pp. 326-333, April 2012.

[9] S. Makino, Y. Konishi, H. Nishikawa, S. Morita, S. Kuroda, and Y. Inasawa, "Far-field RCS prediction from measured near-field data including metal

ground bounce," *21st Annual Review of Progress in ACES*, Honolulu, Hi, 2005.

Pax S. P. Wei received his B.Sc. from the National Taiwan University in 1960, his M.Sc. from University of Illinois in 1963, and his PhD in chemical physics from the California Institute of Technology in Pasadena, CA in 1968. After two years at the Bell Telephone Labs in Murray Hill, NJ, he joined the Boeing Company in Seattle, WA in 1969. There he performed research in low energy electron diffraction (LEED), optical spectroscopy on laser-produced plasmas and electrical discharge, and polarimetric radar target signature analysis. Dr. Wei started to work on RCS measurements from 1991; his interest was in radar response from simple geometric shapes for calibration and uncertainty analysis. He retired from the Boeing Company in 2010.